

We are IntechOpen, the world's leading publisher of Open Access books Built by scientists, for scientists

4,800

Open access books available

122,000

International authors and editors

135M

Downloads

Our authors are among the

154

Countries delivered to

TOP 1%

most cited scientists

12.2%

Contributors from top 500 universities



WEB OF SCIENCE™

Selection of our books indexed in the Book Citation Index
in Web of Science™ Core Collection (BKCI)

Interested in publishing with us?
Contact book.department@intechopen.com

Numbers displayed above are based on latest data collected.
For more information visit www.intechopen.com



Chapter

Influence of Landsat Revisit Frequency on Time-Integration of Evapotranspiration for Agricultural Water Management

Ricardo Trezza, Richard G. Allen, Ayse Kilic, Ian Ratcliffe and Masahiro Tasumi

Abstract

The objective of this study was to explore the improvement in accuracy of estimates for evapotranspiration (ET) over complete growing seasons and monthly periods, when more frequent Landsat imagery is made available. Conversely, we explored the reduction in accuracy in ET estimates when frequency of Landsat imagery was reduced. The study was implemented by conducting a series of METRIC applications for two Landsat WRS path overlap areas, one in southern Idaho (paths 39 and 40) during 2000, and a second one in Nebraska (paths 29 and 30) during 2002, years when two fully functioning satellites, Landsat 5 and Landsat 7, were in orbit. The results indicated that high frequency imagery provided by two satellites covering a WRS path overlap was more able to capture the impacts of rapid crop development and harvest, and evaporation associated by wetting events. That data set simulated a nominal four-day revisit time. Three-simulated 16-day revisit data sets created using a single Landsat series for a single path were unable to produce monthly and growing season ET due to the lack of sufficient number of images to even begin the time-integration process. This emphasizes the need to maintain two Landsat satellites in orbit and the high value of four-day revisit times. Limiting the data set to one path and two satellites (eight-day revisit) underestimated growing season ET accordingly by about 8% on average. Error in monthly ET was relatively high when image availability was limited to that for an eight-day revisit. This is due to the importance of timing of images to identify key inflection points in the ET_F curves and to capture special events such as wetting events from irrigation and rain or from water stress or cuttings, as in the case of forage crops. Results suggest that a four-day revisit time as represented by the full-run (run 1) of our analysis provides robustness in the development of time-integrated ET estimates over months and growing seasons, and is a valuable backstop for mitigation of clouded images over extended periods.

Keywords: evapotranspiration, remote sensing, METRIC, LANDSAT, temporal resolution

1. Introduction

Evapotranspiration (ET) transfers large volume of water from soil and vegetation into the atmosphere. Quantifying the consumption of water over large

areas and within irrigated projects is important for solving water right disputes, hydrologic water balances, and water resources planning. Estimation of actual ET at relatively high spatial resolutions is of interest to agriculture, water resources management, and can serve as an indicator of crop water deficits.

With the availability of free satellite imagery, especially Landsat, there has been substantial investigation to retrieve actual evapotranspiration (ET) over large areas from remotely sensed data. The major advantage of applying remote sensing is that ET can be computed directly without the need for quantifying other complex hydrological processes. A detailed review of remote sensing algorithms to estimate ET are presented in Kustas and Norman [1], Bastiaanssen [2], Courault et al. [3], and Kalma et al. [4]. There are two general approaches to estimate ET via remote sensing: (a) scaling ET based on a vegetation index [5, 6] and (b) using thermal information to drive a surface energy balance [7, 8] or to more simply scale the ET values [9]. The thermal approach is the only one that can effectively estimate ET from water-stressed vegetation as well as evaporation from wet soil when using a surface energy balance [10]. The estimation of ET implies the use of remotely sensed spectral data, thermal imagery, and ground-based meteorological inputs to evaluate net radiation (R_n), sensible heat (H), and soil heat flux (G) components of the surface energy balance to obtain latent heat flux (LE) as the residual from the energy balance. Some information is commonly supplied by a soil water balance [10].

Many applications in water resources planning, hydrological modeling, and agricultural water management require seasonal/annual ET estimates. The determination of seasonal ET based on remote sensing data is very challenging when daily ET is not available due to temporal resolution of satellites (revisiting) and/or gaps in image acquisition due to cloud cover. The methods discussed in the previous paragraph are useful to estimate ET for the days when cloud-free satellite imagery is available, which generally represents just a small portion of the total number of days during the growing season. For that reason, methods are needed to extrapolate and/or interpolate those ET snapshots to represent the whole growing season.

One approach for estimating monthly and seasonal ET from a given number of satellite-derived ET maps is based on the construction of a crop coefficient curve, for every pixel, similar to the proposed by FAO-56 [11]. In this approach, satellite-derived ET is converted to alfalfa reference ET fraction ($ET_{rF} = ET/ET_r$) or grass reference ET fraction ($ET_{oF} = ET/ET_o$) by dividing ET to alfalfa reference evapotranspiration (ET_r) or grass reference evapotranspiration (ET_o), respectively. Basically, each ET image would provide one point of the ET_{rF} or ET_{oF} curve. The rest of the curve is later completed by interpolation (linear, spline, or other method), providing ET_{rF} (or ET_{oF}) for every day during the growing season. Finally, daily ET_{rF} (or ET_{oF}) is multiplied by daily ET_r (or ET_o) to produce daily ET, which can be summarized into monthly and seasonal values.

Allen et al. [12] used METRIC [13] and interpolation of daily alfalfa reference ET fraction (ET_{rF}) for computing seasonal ET in Southern Idaho. This approach resulted in less than 3% difference on seasonal ET when compared to lysimeter data [11]. The authors attributed this good estimation of seasonal ET to the random distribution of daily ET from the METRIC model. Chavez et al. [14] used interpolation of grass reference ET fraction (ET_{oF}) to estimate ET in between satellite overpasses.

Singh et al. [15] employed three different methods of ET_{rF} interpolation to compute seasonal ET for 6 months (July–December) and compare these values with daily ET measurements collected with eddy covariance in Nebraska. The first method assumed that ET_{rF} on each acquired image date was constant during a representative period for daily ET computation. The second method involved linear

interpolation of ET_rF in between two consecutive images; the hypothesis here was that the errors caused by underestimation or overestimation of daily ET are canceled out while computing seasonal ET. These methods are convenient if satellite images are available at regular intervals. The third interpolation method used was a cubic spline of the ET_rF values. The spline method is the procedure that better mimic the natural behavior of the crop coefficient curve. The results indicated that there was no statistically significant difference among the three methods; overall, the cubic spline method resulted in the lowest standard error.

Mohamed et al. [16] used SEBAL [17] to describe the temporal variability of ET in swamps of the upper Nile. The authors estimate ET during days with no satellite image by assuming that the daily ratio of daily evaporation and reference evapotranspiration ($K_c = ET/ET_o$) could be kept constant during the month. ET_o represents the grass-based reference evapotranspiration calculated using Allen et al. [11] and ET was calculated using SEBAL.

Bashir et al. [18] used LANDSAT and MODIS imagery to estimate the spatial distribution of daily, monthly, and seasonal ET for irrigated Sorghum in the Gezira scheme, Sudan. The authors used SEBAL to estimate daily ET. The monthly and seasonal ET was computed by linearly interpolating the ratio of ET and grass reference ET_o (ET_oF) in between two consecutive images; the estimation of seasonal ET by SEBAL and ET_oF interpolation was within 8% of an estimation of seasonal ET from water balance.

A second approach that is implemented to generate seasonal or annual ET utilized soil-vegetation-atmosphere transfer (SVAT) models to estimate ET in between satellite dates. Olioso et al. [19] combined remote sensing inputs and a SVAT model to estimate ET and photosynthesis. The authors indicate that is useful to assimilate remote sensing data into SVAT models, which are able to give access to a detailed description of soil and vegetation canopy processes. SVAT models are capable of simulating intermediary variables linked to hydrological and physiological processes. Various remote sensing data may be used to drive those SVAT models. Spectral reflectance in the visible and near infrared portions of the spectrum can provide information on the structure and characteristics of the vegetation canopy, such as LAI and albedo. Thermal remote sensing data can be used as indirect indicators of moisture in the soil or vegetative surface. Dhungel et al. [20] proposed a surface energy balance model that uses gridded weather data to interpolate ET between two consecutive satellite dates; bulk surface resistance for satellite dates was obtained by inversion of the Penman-Monteith equation, where ET came from application of the METRIC model on Landsat images.

1.1 Objective

The objective of this study was to explore the improvement in accuracy of estimates for ET over complete growing seasons and for monthly periods, when more frequent Landsat imagery is made available.

The study was implemented by conducting a series of METRIC applications for a Landsat WRS path overlap area in southern Idaho (paths 39 and 40) during a period (year 2000) when two fully functioning satellites, Landsat 5 and Landsat 7, were in orbit. During that year, Landsat 5 (L5) and Landsat 7 (L7) passed over the overlap area twice, each, per 16 day period, providing four imaging opportunities every 16 days. Monthly and growing season ET was integrated using all available cloud-free imagery during the April–October growing period to provide a baseline representing our most accurate estimate. The frequency of imagery was then sparsened by removing imagery from one path or the other and by removing imagery from one satellite or the other. Monthly and seasonal ETs were then recomputed with the sparsened image series and compared with the baseline data.

1.2 Background

In this chapter, Mapping EvapoTranspiration at High Resolution with Internal Calibration (METRIC) was used to produce ET maps in Idaho and Nebraska using Landsat imagery. METRIC is an image processing model for calculating ET as a residual of the surface energy balance. METRIC was developed by the University of Idaho [7, 8, 16] for the application to Landsat satellite imagery to maximize ET product resolution (30 m). METRIC uses as its foundation, the pioneering SEBAL energy balance process developed in the Netherlands by Bastiaanssen et al. [12, 17], where near surface temperature gradients for estimating the sensible heat component of the surface energy balance are an indexed function of radiometric surface temperature, thereby, eliminating the need for absolutely accurate surface temperature and the need for air temperature measurements. The surface energy balance is inversely and internally calibrated in METRIC using ground-based reference ET to reduce computational biases inherent to remote sensing-based energy balance components and to provide congruency with traditional methods for ET [8]. Slope and aspect functions and temperature lapsing are used in applications in mountainous terrain. The primary inputs to the METRIC model are short wave and long wave (thermal) images from satellite (e.g., Landsat or MODIS), a digital elevation model (DEM), and ground-based weather data measured within or near the area of interest. ET “maps” (i.e., images) via METRIC provide the means to quantify ET on a field-by-field basis in terms of both the rate and spatial distribution.

METRIC has significant advantages over conventional methods for estimating ET from crop coefficient curves in that crop development stages do not need to be known with METRIC, nor does the specific crop type need to be known. In addition, the energy balance can detect reduced ET caused by water shortage. For agricultural crops, METRIC takes significant advantage of basing calibration on reference ET, rather than evaporative fraction [18], where reference ET, in the case of METRIC, is the ET from a hypothetical 0.5 m tall vegetation having high leaf area and low bulk surface resistance. The reference ET is estimated from ground-based weather data using the ASCE standardized Penman-Monteith method for the ‘tall reference’ [19]. The use of reference ET accounts for regional advection effects can cause ET from irrigated and wetland vegetation systems to exceed daily net radiation in many arid or semi-arid locations [16]. Details on the METRIC model are provided in Allen et al. [8].

In the METRIC model, ET is computed from satellite images and weather data using the surface energy balance. Since the satellite image provides information for the overpass time only, METRIC computes an instantaneous ET flux for the image time. The ET flux is calculated for each pixel of the image as a “residual” of the surface energy budget equation and is expressed as the energy consumed by the evaporation process:

$$LE = R_n - G - H \quad (1)$$

where LE is the latent heat flux (W/m^2), R_n is the net radiation flux at the surface (W/m^2), G is the soil heat flux (W/m^2), and H is the sensible heat flux to the air (W/m^2).

ET produced by METRIC is expressed in the form of a reference ET fraction (ET_rF) that is calculated as the ratio of the computed instantaneous ET (ET_{inst}) from a pixel to a reference ET (ET_r) that is computed from weather data:

$$ET_r F = \frac{ET_{inst}}{ET_r} \quad (2)$$

where ET_{inst} is produced from the energy balance of METRIC (mm hr^{-1}) and ET_r is reference ET based on the standardized 0.5 m tall alfalfa reference at the time of the image. ET_r represents a near maximum rate of ET based on environmental energy availability and advection of sensible heat and dry air from outside irrigated areas. Generally, only one or two weather stations are required to estimate ET_r for a Landsat image that measures $180 \text{ km} \times 180 \text{ km}$. $ET_r F$ is same as the well-known crop coefficient, K_c , when used with an alfalfa reference basis, and is used to extrapolate ET from the image time to 24-hour or longer periods because ET_r represents a near maximum limit for ET; $ET_r F$ values produced by METRIC generally range from 0 to 1.0 [20].

1.3 Seasonal evapotranspiration

Monthly and seasonal evapotranspiration “maps” are highly useful for water resources management, including water rights litigation, hydrologic water balances, ground water studies, and irrigation depletion analyses. Generally, these maps are derived from the series of $ET_r F$ images produced by METRIC by interpolating $ET_r F$ between the processed images and then multiplying, on a daily basis, by the ET_r for each day. The ET_r accounts for day-to-day variation in ET caused by weather fluctuations and the interpolated $ET_r F$ from METRIC accounts for the scaling of the weather-based ET according to the effects of vegetation cover, soil water stress, and other localized factors. As mentioned before, the interpolation of $ET_r F$ between image dates is not unlike the construction of a seasonal K_c curve, where interpolation is done between discrete values for K_c .

Cumulative ET for any period, for example, a month, season, or year is calculated as:

$$ET_{\text{period}} = \sum_{i=m}^n [(ET_r F_i) (ET_{r24i})] \quad (3)$$

where ET_{period} is the cumulative ET for a period beginning on day m and ending on day n , $ET_r F_i$ is the interpolated $ET_r F$ for day i , and ET_{r24i} is the 24-hour ET_r for day i . Units for ET_{period} are in mm, when ET_{r24} is in mm d^{-1} . The interpolation between values for $ET_r F$ is generally made using a curvilinear interpolation function, for example, a spline function, to follow the typical curvilinearity of ET due to the phenological development of crops during the growing season [25].

As a general rule of thumb, one clear satellite image per month is normally considered sufficient to construct an accurate $ET_r F$ curve for purposes of integrating ET over time to estimate seasonal ET. During periods of rapid vegetation change, however, a more frequent image interval is highly desirable, as illustrated in **Figure 1**, where the lack of satellite image in mid-July caused an underestimation of the $ET_r F$ curve for the dry bean crop in Idaho near the beginning of the midseason, when $ET_r F$ was interpolated linearly between satellite dates.

If a specific pixel must be masked out of an image because of cloud cover, then a subsequent image date must be used during the interpolation and the estimated $ET_r F$ or K_c curve will have reduced accuracy. In actuality, $ET_r F$ varies substantially from day-to-day due primarily to variability in weather data and surface wetness. Therefore, the continuous $ET_r F$ curve, whether constructed from a published curve or table, or estimated from METRIC, is only an approximation of the actual $ET_r F$ on any specific day.

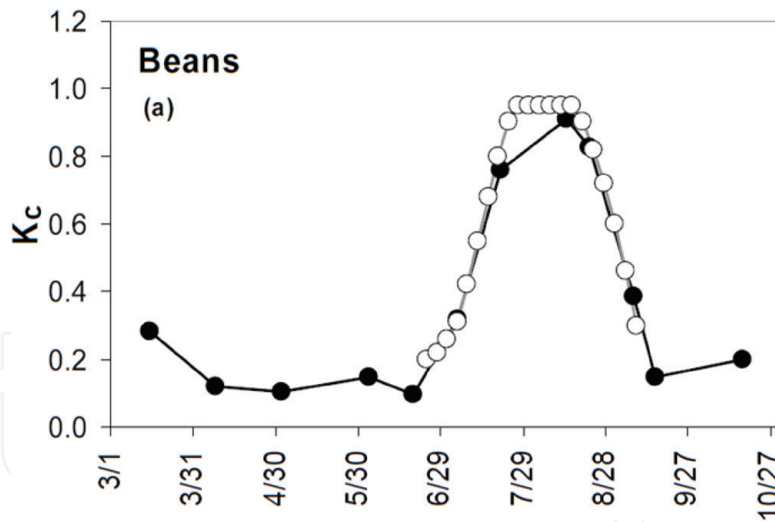


Figure 1. Constructed K_c (or $ET_{r,F}$) curve for a bean crop from METRIC (dark symbols) with comparison against a standard K_c curve produced by the US Bureau of Reclamation Agrimet service for a region near Twin Falls, Idaho in year 2000.

2. Methods and materials

2.1 Study areas

Two application areas were utilized for this test. One area was in southern Idaho and the second area was in central Nebraska. Idaho is a relatively ‘clear’ area, so that, this analysis represents a somewhat ‘optimistic’ scenario as compared to more cloud-prone parts of the USA, for example, the Midwestern states. Central Nebraska has relatively high amounts of cloud cover and presents a greater challenge in obtaining a sufficient temporal density of clear imagery to produce accurate time-integrated estimates of ET.

In both areas, a subarea of Landsat images located in a WRS path overlap was selected for study. In Idaho, the subarea resided within path 39 row 30 and path 40 row 30. The area is shown in **Figure 2**, where the dimensions of the study area were approximately 50 km east–west \times 80 km north–south. The study area contained a mixture of irrigated agriculture comprised of potatoes, sugar beets, alfalfa, peas, dry beans, corn, small grains (wheat and barley), and pasture surrounded by areas of sagebrush desert with some grasslands. The upper part of the study area contains basaltic flows from the Craters of the Moon National Monument and some mountainous terrain lies to the south. Annual precipitation

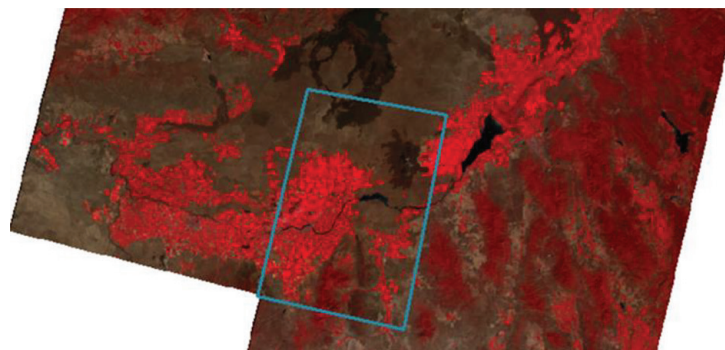


Figure 2. Idaho study area, outlined in blue, that lies in the overlap of Landsat WRS paths 40 (on the left) and 39 (on the right) overlaid onto a false color composite from Landsat 7 on August 14, 2000 for path 40 and Landsat 5 on June 28, 2000 for path 39. Irrigated areas along the Snake River plain are shown as bright reds.

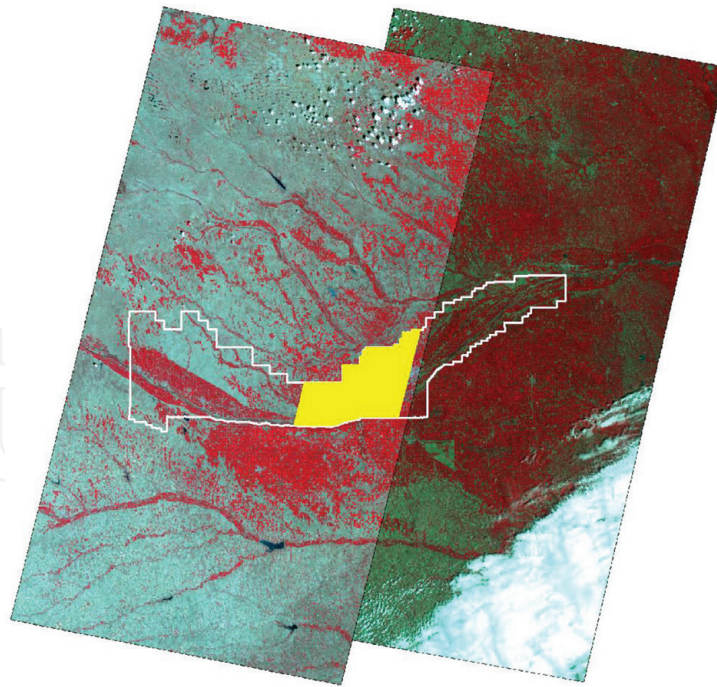


Figure 3. Nebraska study area shaded in yellow where path 29, rows 30–31 and path 30, rows 30–31 overlap. The area managed by Central Platte NRD is outlined in white. The images shown are false color composites from Landsat 7 on July 29, 2002 for path 29 and Landsat 7 on July 22, 2002 for path 30.

is about 200 mm and all agricultural crops are irrigated from surface water or from ground water.

In Nebraska, the subarea resided within the domain of the Central Platte Natural Resources District (NRD) that lies within the overlap of WRS path 30 rows 30–31 and path 29 rows 30–31. That study area in central Nebraska is shown in **Figure 3** and has dimensions of approximately 60 km by 50 km with an area of approximately 1900 km². Corn and soybeans are the predominant agricultural crops grown in this section of Nebraska, with some alfalfa cultivation as well. Agricultural irrigation is important to this area with over 18,000 irrigation wells and over 1 million certified irrigated acres. The dominant irrigation method in the area is center pivot and the irrigation season generally lasts from mid-June to mid-September. Annual precipitation for this area is approximately 600–650 mm. **Figure 4** shows a close-up of the Nebraska study area showing the distribution of irrigated fields.

2.2 Remote sensing data

Table 1 lists the selection of Landsat images used to time-integrate ET in the Idaho study area. Dates for both path 39 and 40 are listed as well as the Landsat platform that collected the images. Year 2000 was selected for the analysis because it was during a ‘golden period’ of Landsat imagery, where two fully functioning satellites were in operation. Year 2000 was also a year that had previously been processed using METRIC so that those results were available for use in this analysis. Asterisks in **Table 1** indicate the dates used in a particular integration run to estimate monthly and growing season ET. The application of METRIC to the two paths for year 2000 is described in Allen et al. [12] and Trezza [8]. Most of the images listed in **Table 1** were essentially clear images for the small study area and did not require mitigation for clouds. The exception was August 23, 2000 that was half-cloud covered. That image cloud mask was used with the spline model to signal the need to expand the spline to an additional image date. There were a few clear images for the study area

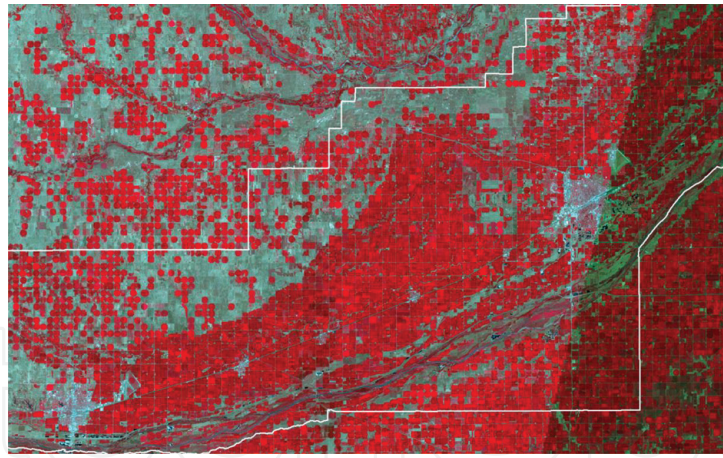


Figure 4. Close-up view of the Nebraska study area extent. The white line is the Central Platte NRD boundary. Bright red areas are cultivated fields and the lighter areas are rangeland. The areas of high densities of fields are irrigated areas along the Platte River, which is visible along the southern boundary of the Central Platte NRD. Those fields utilize a combination of ground water and surface water. Areas of more sparse densities of irrigated fields are fields using primarily ground water a water source.

that had not been processed by METRIC due to the close coincidence of other clear images in time. An example is June 28, 2000 for path 39, which was not processed. Therefore, the list of images in **Table 1** is not all inclusive. However, the absence of images should not impact the accuracy of the baseline estimation of time-integrated ET because there are sufficient data points to afford a relatively accurate interpolation.

Table 2 lists the selection of Landsat images used to time-integrate ET in the Nebraska study area. As with the Idaho study area, year 2002 was selected for analysis because it was a year when both Landsat 5 and 7 satellites were in operation and fully functioning. Asterisks in **Table 2** indicate dates that they were used in a particular integration run to estimate monthly and growing season ET.

Most of the imagery listed were clear images for the small study area and did not require mitigation for clouds. The exceptions were June 27, 2002 and August 6, 2002 from path 30, with both images having significant cloud cover over the study area. Cloud-covered areas in the imagery were masked out by manually tracing around the cloud areas and filling those cloud areas with a value recognizable in the time-integration models as invalid. The masked out areas were replaced with data from a previous or following image date during the spline function in the time-integration.

2.3. Calculation of seasonal ET

The splining of $ET_r F$ between image dates was done using an ERDAS Modelmaker code that implemented a standard cubic spline algorithm. The spline function produced a continuous curvilinear function for each pixel between each date that was continuous in both first and second derivatives. The function intersected each pixel data point. Daily reference ET (ET_r) for the splining was computed from daily weather data obtained from the Twin Falls, Idaho Agrimet automated weather station for year 2000 for the Idaho study. For Nebraska, daily ET_r was computed using hourly weather data from the 23 weather stations obtained from the High Plains Regional Climate Center (HPRCC) Automated Weather Data Network (AWDN), where a daily ET_r surface was computed using cubic spline interpolation. In all cases, ET_r was calculated using the ASCE (2005) standardized Penman-Monteith alfalfa reference ET equation [21–24], and that same equation had been originally used to calibrate the METRIC model during the production of $ET_r F$.

	Dates	Sensor	Run 1: Time integration using both paths and landsats	Run 2: Time integration using path 39 and both landsats**	Run 3: Time integration using path 40 and both landsats	Run 4: Time integration using path 40 and landsat L5***
1	April 01, 2000	L7	*	*		
2	April 08, 2000	L7	*		*	
3	May 02, 2000	L5	*		*	*
4	May 03, 2000	L7	*	*		
5	June 03, 2000	L5	*		*	*
6	June 04, 2000	L7	*	*		
7	June 19, 2000	L5	*		*	*
8	June 20, 2000	L7	*	*		
9	July 05, 2000	L5	*		*	*
10	July 21, 2000	L5	*		*	*
11	July 22, 2000	L7	*	*		
13	August 07, 2000	L7	*	*		
14	August 14, 2000	L7	*		*	
15	August 22, 2000	L5	*		*	*
16	August 23, 2000	L7	*	*		
17	September 07, 2000	L5	*		*	*
18	September 08, 2000	L7	*	*		
19	September 15, 2008	L7	*		*	
20	September 16, 2000	L7	*	*		
21	October 17, 2000	L7	*		*	

*Asterisks indicate the dates used in a particular integration run to estimate monthly and growing season ET. ** In this run, two synthetic ET_rF images were created using constant values and placed at dates November 01, 2000 (ET_rF = 0.25) and November 10, 2000 (ET_rF = 0.1) to provide endpoints for the cubic spline.*

**** In this run, four synthetic images were created using constant values and placed at dates March 20, 2000 (ET_rF = 0.1); March 31, 2000 (ET_rF = 0.1); November 01, 2000 (ET_rF = 0.25) and November 10, 2000 (ET_rF = 0.1) to provide endpoints for the cubic spline.*

Table 1.
Selection of Landsat images used to time-integrate ET for the Idaho study area, showing collection path and platform.

	Dates	Sensor	Run 1: Time integration using both paths and landsats	Run 2: Time integration using path 30 and both landsats	Run 3: Time integration using path 29 and both landsats	Run 4: Time integration using path 29 and landsat L5	Run 5: Time integration using path 29 and landsat L7
1	April 24, 2002	L7	*	*			
2	May 02, 2002	L5	*	*			
3	May 03, 2002	L7	*		*		*
4	June 11, 2002	L7	*	*			
5	June 27, 2002	L7	*	*			
6	June 28, 2002	L5	*		*	*	
7	July 22, 2002	L7	*		*		*
8	July 29, 2002	L7	*	*			
9	July 30, 2002	L5	*		*	*	
10	August 6, 2002	L5	*	*			
11	August 14, 2002	L7	*	*			
13	August 15, 2002	L7	*		*		*
14	August 23, 2002	L7	*		*		*
15	August 31, 2002	L5	*		*	*	
16	September 7, 2002	L5	*	*			
17	September 8, 2002	L7	*		*		*
18	September 15, 2002	L7	*	*			
19	September 16, 2002	L5	*		*	*	
20	September 23, 2002	L5	*	*			

Asterisks indicate the dates used in a particular integration run to estimate monthly and growing season ET.

Table 2.
Selection of Landsat images used to time-integrate ET for the Nebraska study area, showing collection path and platform.

Three to four integration runs were made for the study areas, as described in the next section. The integration runs utilized (1) both Landsat 5 and 7 imagery from both paths; (2) both Landsat 5 and 7 imagery from one path or the other; and

(3) imagery from only one Landsat 5 from one path only. The first integration run approximated a condition, where four images are collected each 16 days. This is a condition that would occur with four Landsat satellites in orbit with the current path width or with two Landsat satellites in orbit, each having a 'double-wide' path of approximately 300 km. The second and third integration runs approximated the condition where two currently formulated Landsats are in orbit at any one time, for the center of a WRS path. The last condition represents the condition, where only one Landsat satellite is in orbit.

In the Idaho study area, ET was integrated over the April 1–October 31 period to form monthly ET for April through October. The absence of clear images for the study area during late March and early April and during late October and early November for some of the time integration runs required the use of 'synthetic' images to represent ET conditions during these periods. The synthetic images were required to anchor the spline function prior to April and following October. The synthetic images were created for the Idaho study area by applying a daily soil water balance model for a bare soil condition [11] representing surface conditions during Idaho winters and late falls, where nearly all vegetation is dormant due to freezing. The daily soil water balance model used the FAO-56 evaporation model [11] and was applied to 18 weather stations in the region and an evaporation surface was created using inverse distance interpolation. The average $ET_{r,F}$ during the late March to early April and from late October to early November periods was determined by averaging the simulated evaporation rates over those periods. Those synthetic images were then used as beginning and ending points for the spline interpolation process.

No synthetic images were required for the full two-Landsat/two-path integration for the Idaho study area, as sufficient image dates during early April and late October were available. In the double satellite/single path integration, however, synthetic $ET_{r,F}$ images were required at the end of the growing season to provide endpoints for the cubic spline, and were placed on dates November 01, 2000 ($ET_{r,F}$ averaged 0.25) and November 10, 2000 ($ET_{r,F}$ averaged 0.1). For the run using only Landsat 5 data and for path 40 only, synthetic images were required at both the beginning and end of the growing season. In this run, four synthetic images were placed on dates March 20, 2000 ($ET_{r,F}$ averaged 0.1); March 31, 2000 ($ET_{r,F}$ averaged 0.1); November 01, 2000 ($ET_{r,F}$ averaged 0.25); and November 10, 2000 ($ET_{r,F}$ averaged 0.1) to provide endpoints for the cubic spline.

For the Nebraska study area, ET was integrated over the May–September period, representing the shorter growing season for the predominately corn and soybean crop rotation there, as opposed to the April–October growing period for Idaho crops. As with Idaho, $ET_{r,F}$ for bare soil was also estimated for the Nebraska study area using the FAO-56 style evaporation model for the purpose of creating synthetic images for April 1, April 15, October 15, and November 15. These dates and synthetic images were used in each of the time-integration analyses to approximate ET conditions during those general periods so that the spline function could be applied with spans covering May–September.

In both study areas, about 1500 data points were sampled. The points were selected from the interiors of irrigated fields, with one point per field. Pixels were located far from field edges to avoid contamination of thermal pixels from thermal information from outside the field. Nearly all of the Idaho sample locations were in agricultural fields, with about 15 sample points taken from desert rangeland. Irrigated agriculture was emphasized in this study due to its importance in water resources management. In the Nebraska data set, about 100 sample pixels were selected from rangeland and riparian areas each. The rest were from irrigated agriculture.

2.4 Model runs

The first baseline model runs used all 21 ET_rF images listed in **Table 1** for Idaho and all 20 images listed in **Table 2** for Nebraska. These runs, representing a condition with four traditional Landsat satellites in orbit or two ‘double-wide’ Landsats providing four images every 16 days, served as baselines for comparing against sparser image data sets. There were seven times in Idaho and six times in Nebraska when image dates were only 1 day apart, as shown in **Tables 1** and **2**, due to the scheduling of the two Landsat systems and geometry of the WRS path system. In cases where images were 1 day apart, we subtracted 2 days from the first image and added 2 days to the second image in the baseline spline model run 1. This was required to keep the spline function from creating large vertical components caused by a time difference of only 1 day. In cases where images were 1 day apart, the additional information afforded by the second image was deemed to be of much less value than if it had been 4 days apart. Four days apart, larger changes would have occurred in ET_rF due to vegetation development and wetting conditions in addition to larger differences in cloudiness. Images 1 day apart typically had similar cloud conditions and ET_rF behavior.

Four other integration runs were carried out for the Idaho study area as indicated in **Table 1**. These runs represented conditions where fewer than four revisits per 16-days were available. Runs 2 and 3 were made using Landsat 5 and Landsat 7 images from only one path, either path 39 or path 40. These runs represent scenarios where two Landsat satellites are in orbit and the focus includes the center two-thirds of a path so that the revisit time is each 8 days. Runs 2 and 3 represent two replicates of the same scenario of 8 day revisit, which is possible in the path overlap area.

Run 4 for the Idaho study represents the scenario presented when only one Landsat is in orbit, collecting data every 16 days. This represents the actual scenario for the USA during the late 1980s and 1990s when only Landsat 5 was collecting data and again in 2012 when only Landsat 7 was collecting data. Run 4 was constructed by using imagery for path 40 and Landsat 5. Additional runs 5, 6, and 7, would have represented three additional replicates of a single satellite having 16-day revisit, via combinations of path 40 with Landsat 7 and path 39 with Landsat 5 and path 39 with Landsat 7. However, runs 5, 6, and 7 were not possible to implement because too few images were available during the April–October to apply the ET_rF interpolation process without applying what was considered to be too much speculation on the evolution and trends in ET_rF over time.

Nebraska runs 2 and 3 were made using a combination Landsat 5 and Landsat 7 images from only path 30 or from only path 29. These runs represent scenarios, where two Landsat satellites are in orbit so that the revisit time is each 8 days. Model runs 4 and 5 applied Landsat 5 and Landsat 7, respectively, to path 29, only. Each of these runs represented conditions where only a single Landsat is in orbit, with revisit of 16 days for the majority of a path area. This represents the actual scenario for the USA during the late 1980s and 1990s when only Landsat 5 was collecting data and again in 2012 when only Landsat 7 was operational. Model run 4 was setup to only process imagery from Landsat 5 for path 29 and model run 5 was setup to only process imagery from Landsat 7 for path 29.

3. Results

3.1 Splining results

Figures 5 and **6** are examples of daily ET_rF curves for the April–October period in Idaho created by the spline interpolation process for 20 sample locations

representing 20 agricultural fields and crops. The ET_rF curves represent the anticipated ET_rF on any given day, given the ET_rF information input to the splining process. Three of the integration runs are plotted in the figures: the full base run (run 1) containing 21 ET_rF data points from 21 image dates, run 2 representing a two-Landsat system in the middle of a WRS path having an eight-day revisit schedule, and run 4 representing a one-Landsat system in the middle of a WRS path having a 16-day revisit schedule. Run 2 contained 9 ET_rF data points from 9 image dates and run 4 contained only 7 ET_rF data points from 7 image dates. The ET_rF curves, which represent the ratio of actual ET to the ASCE Penman-Monteith-based reference ET, are characteristic of crops grown in southern Idaho, where ET_rF is relatively low during spring prior to vegetation development, when most ET stems from evaporation from wet soil. ET_rF increases during late spring and early summer toward 1.0, representing near maximum ET rates from vegetation that fully covers the ground, and then decreases during fall as crops mature and die or are harvested.

Some of the ET_rF curves in **Figures 5 and 6** exhibit impacts of evaporation from late summer irrigations following harvest of crops. This is a typical cultural practice

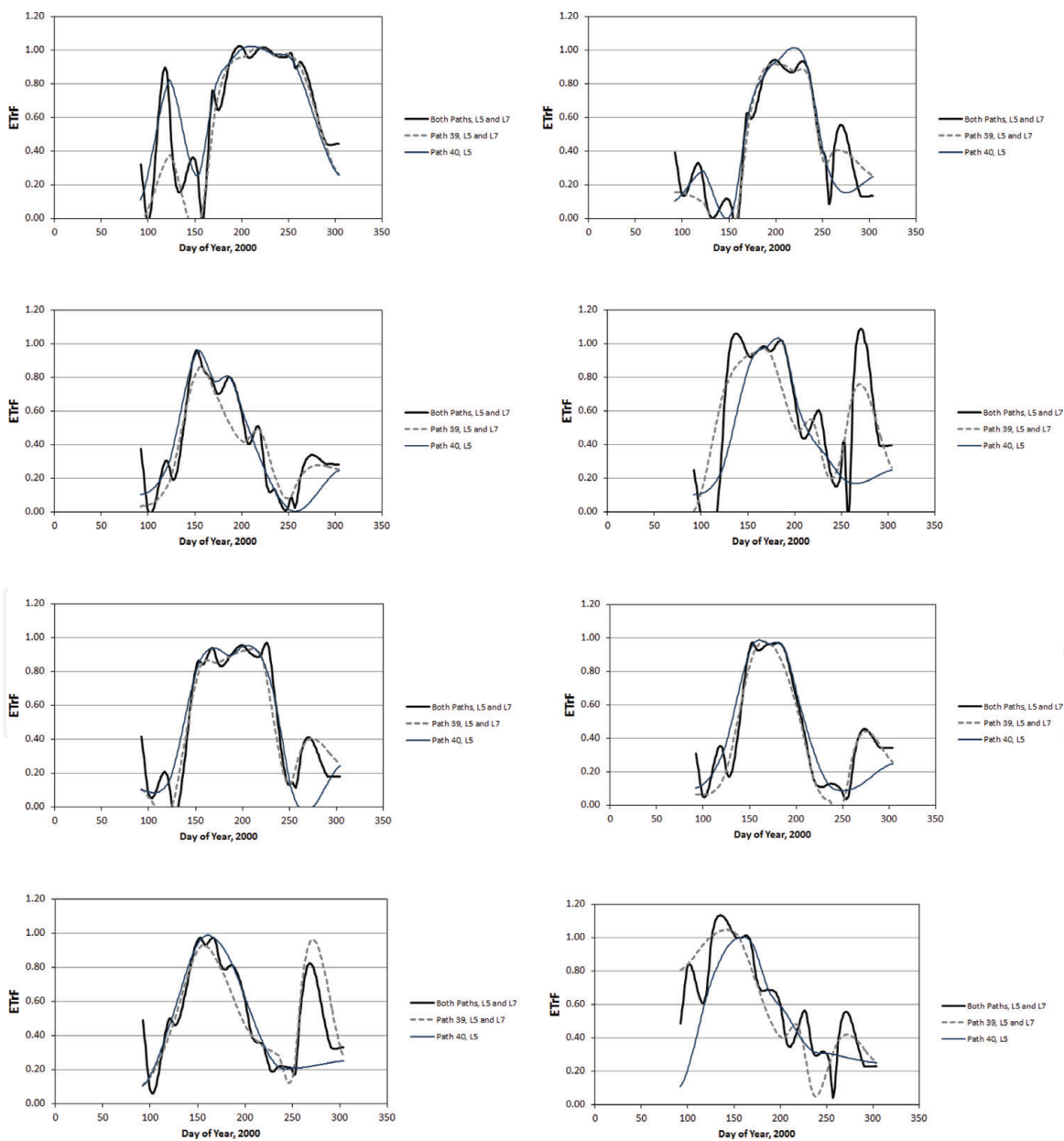


Figure 5. About 10 representative ET_rF curves for the southern Idaho analysis area during year 2000 created by cubic spline interpolation of ET_rF for runs 1, 2, and 4.

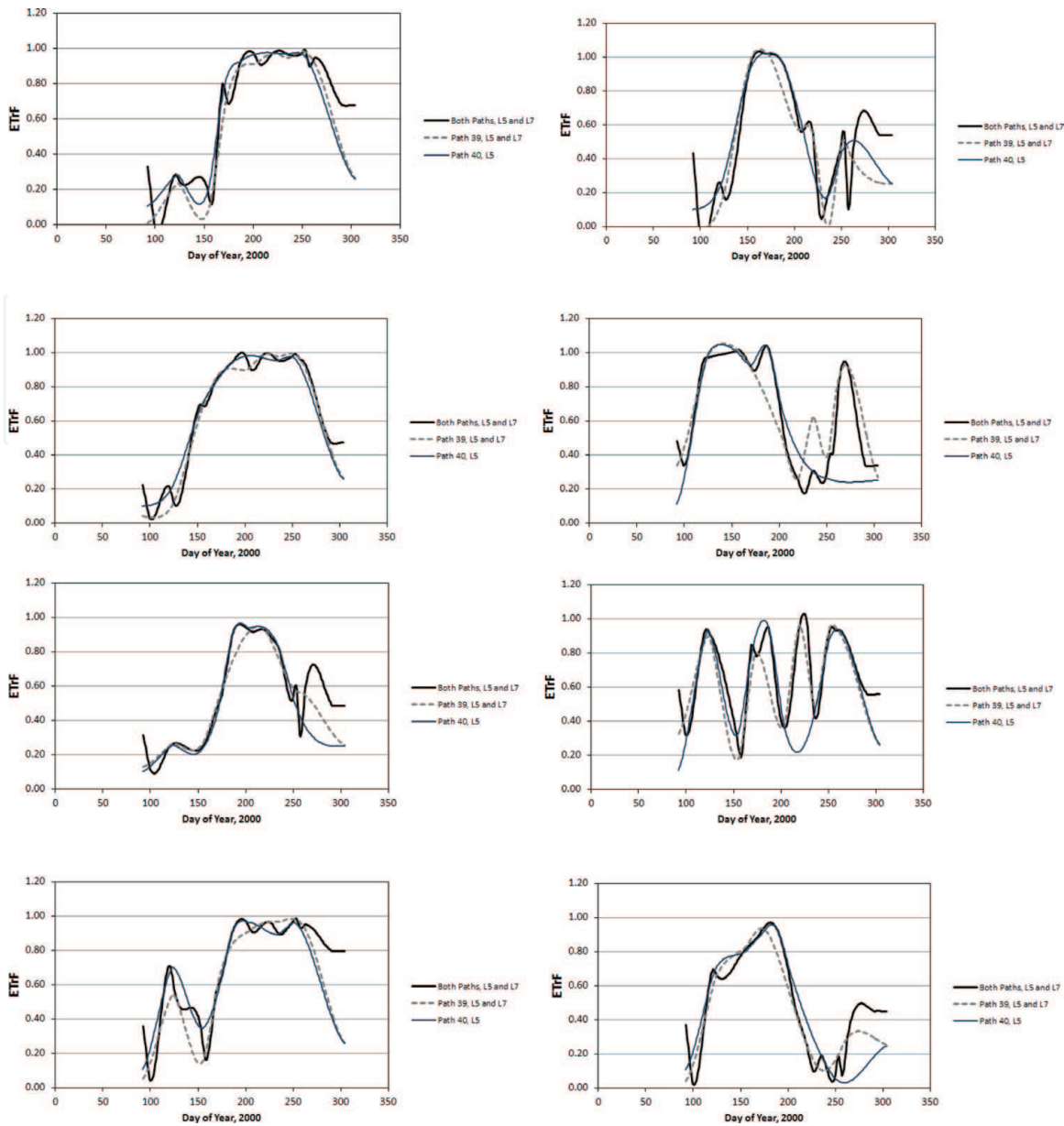


Figure 6. About 10 additional representative ET_rF curves for the southern Idaho analysis area during year 2000 created by the cubic spline interpolation of ET_rF for runs 1, 2, and 4.

in Idaho. Other curves reflect behavior for alfalfa crops that are harvested three to five times per growing season so that the ET_rF curves fluctuate up and down over time. The higher frequency imagery in run 1 was able to capture more of the impacts of harvest and regrowth of alfalfa on the ET_rF values. Both runs 2 and 4 missed some of the alfalfa regrowth cycles, for example in the top right graph in **Figure 6**. Run 4 with only 7 image dates generated smoother ET_rF curves due to the more sparse data points. The smoother curves tended to average out variation in ET_rF caused by variation in water availability or variation in evaporation from soil following irrigation or precipitation wetting events.

3.2 Monthly comparisons

Idaho: Example plots of ET integrated over months of April and July are shown in **Figure 7** for the Idaho study area, where ET from runs 2 and 3 is plotted against ET from run 1. Data for 1500 fields are shown. Limiting the image collection to one path for two satellites reduced the number of images available to the spline and impacted the monthly integrations.

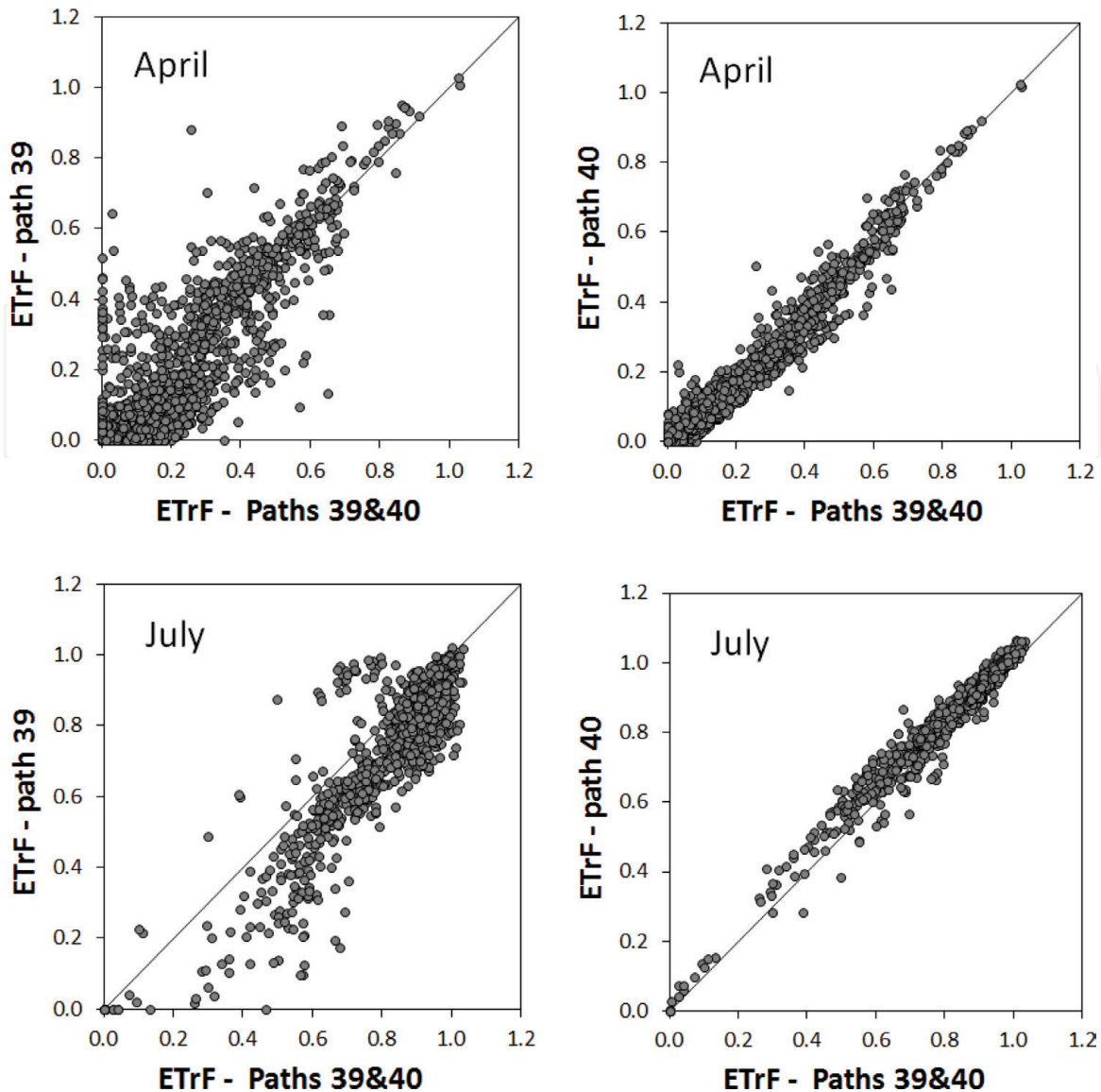


Figure 7. Monthly ET_rF produced by time-integration from run 2 (left column) and run 3 (right column) versus ET_rF produced from the baseline run 1 for the southern Idaho analysis area during year 2000.

Run 3 used images from path 40 and agreed closest with the two-path integration due to the stronger influence of path 40 in the two-path product. Images from path 39 exhibited more dryness for fields having relatively low amounts of vegetation cover in the July time frame, due to fewer rain events prior to those images. This manifested as lower ET_rF for run 2 that was based on path 39 images versus the baseline run 1 for July for fields having low ET_rF .

Monthly ET averaged over the 1500 sample points is plotted in **Figure 8** and monthly ET_rF is plotted in **Figure 9**. In general, although ET and ET_rF for some fields deviated relatively widely between runs, as shown in **Figure 7**, and which would be a concern for those individual water rights holders, ET and ET_rF averaged over a large number of fields yielded relatively similar and consistent values.

Nebraska: Example plots of ET integrated over months of May, June, July, and August are shown in **Figures 9–12** for the Nebraska study area, where ET from runs 2, 3, 4, and 5 are plotted against ET from baseline run 1. Data for 1500 fields are shown. As with the Idaho analyses, limiting the image collection to one path for two satellites reduced the number of images available to the spline and substantially impacted the monthly integrations. For the month of May, ET estimated using only imagery from one path estimated as much as 40% higher

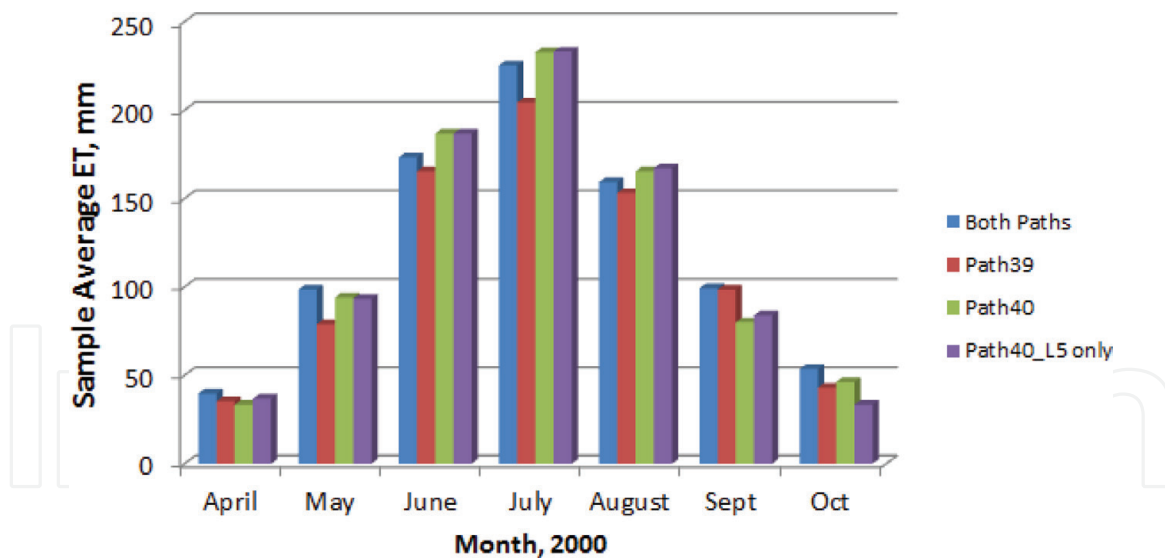


Figure 8.

Monthly ET averaged over the 1500 sampled locations for the Idaho study area for the four time-integration runs that used all available images in both paths, images from path 39 only, images from path 40 only, and images from path 40 and Landsat 5, only.

than the baseline ET. The cause of the differences was differential wetness of images due to rainfall for the collections on the two paths as well as longer spans between images in the spline integration and reliance on image information further away in time.

For example, large differences in $ET_{r,F}$ existed between the May 2, 2002, path 30 image and the May 3, 2002, path 29 image due to rapid drying of soil between the two date and probable differences in calibration of the METRIC model for the two dates for low vegetation conditions (**Figure 5**). Comparison of golf courses and agricultural fields with full cover between the images yielded similar values, indicating similar calibration for those conditions. The Ord AWDN station, approximately 50 km north of the study area, recorded 22 mm of precipitation on May 27, 2002 and 5 mm on May 1, 2002. The Halsey AWDN station, approximately 100 km from the study area, recorded 19 mm on April 27, 2002 and 12 mm on May 1, 2002. The higher $ET_{r,F}$ for the path 30 image caused time-integrated ET for the month of May to be higher than for path 29 when each path was processed alone.

The large difference in $ET_{r,F}$ between the 5/2 and 5/3 image dates also may have affected the accuracy of the spline function when applied to the baseline run 1. The large differences in $ET_{r,F}$ and the closeness in time between the images may have caused the spline function to produce overly high or low $ET_{r,F}$ values for periods between image dates. This may have occurred even though all images that were only 1 day apart had their dates spaced 5 days apart during the splining process in an attempt to avoid the large slopes in the spline. The plot of $ET_{r,F}$ for path 29 using only Landsat 5 had greatest deviation from the baseline run due to the lack of cloud-free imagery for Landsat 5 on path 29 in May. Therefore, the splining process relied on $ET_{r,F}$ data from the synthetic images spaced in April and $ET_{r,F}$ data from the month of June.

Comparisons of $ET_{r,F}$ improved for June for the Nebraska study area, as shown in **Figure 12**, where the same runs as for **Figure 10** are shown. Poorest agreement in monthly $ET_{r,F}$ values for June occurred for path 29 only using Landsat 7 only due to no available clear images in June, and therefore the need to interpolate across a large time span. Although comparisons approved between the various runs and the baseline runs for June, large differences still occurred, which is of concern for water accounting or ET sampling processes that require knowledge

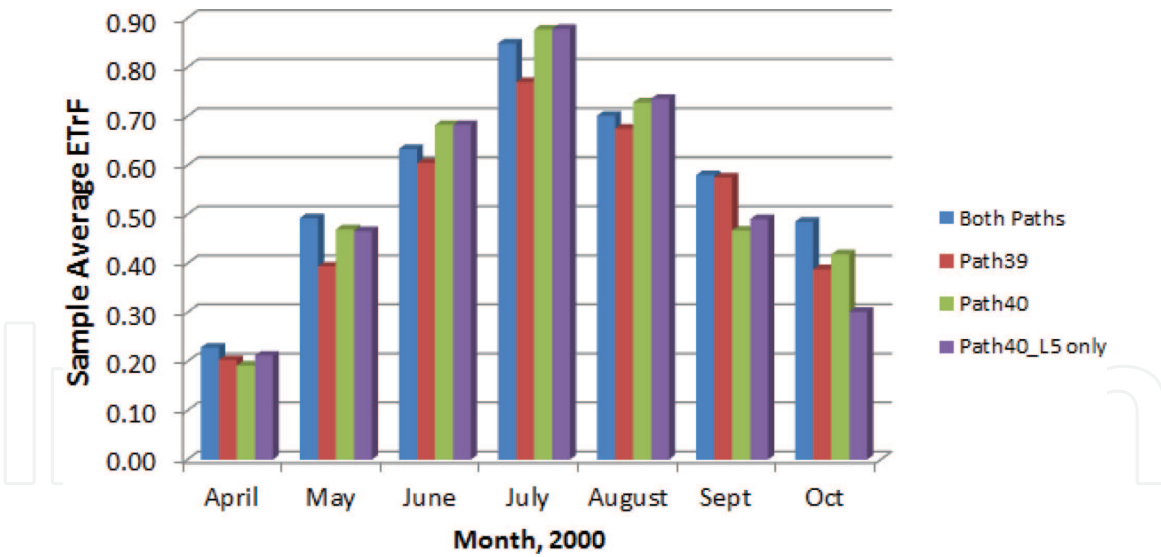


Figure 9. Monthly ET_rF averaged over the 1500 sampled locations for the Idaho study area for the four time-integration runs that used all available images in both paths, images from path 39 only, images from path 40 only, and images from path 40 and Landsat 5, only.

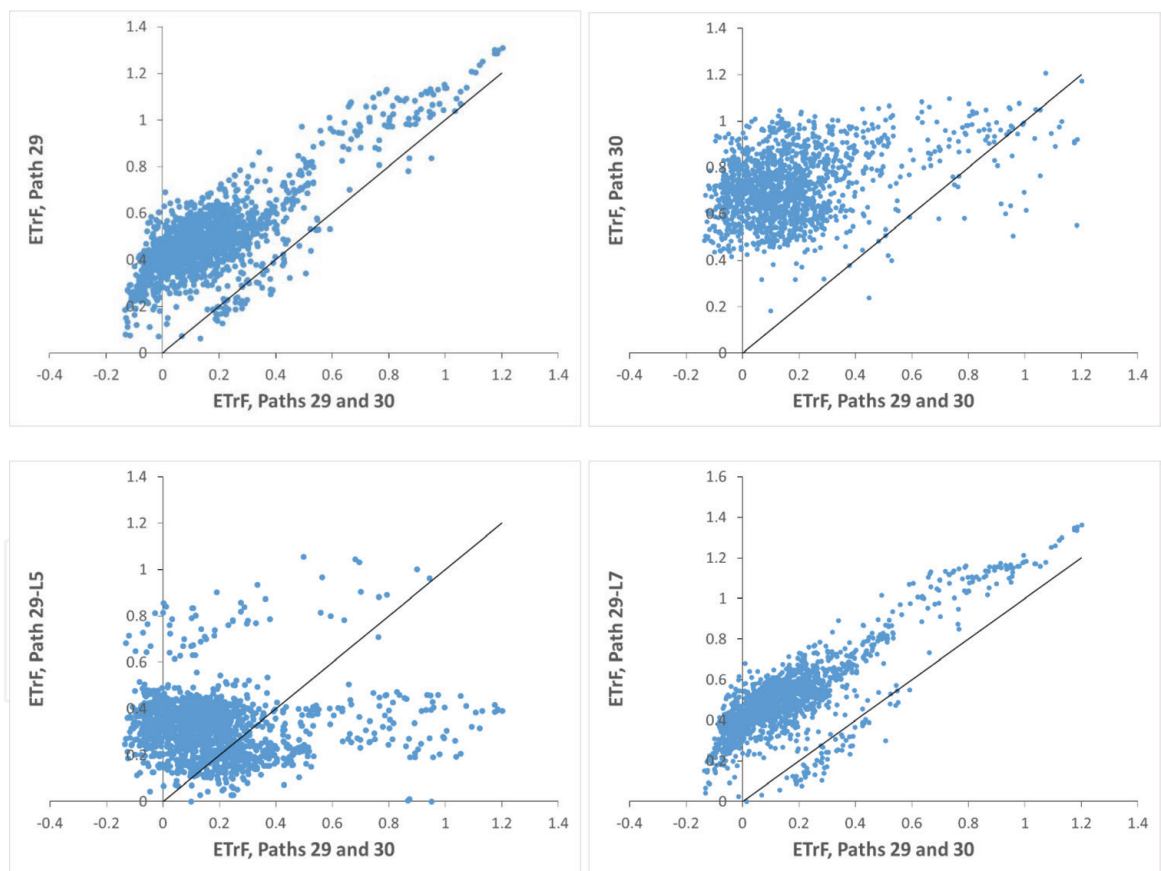


Figure 10. Plots of average integrated ET_rF for May from model run 2 (two Landsats on path 29), run 3 (two satellites on path 30), run 4 (Landsat 5, only on path 29), and run 5 (Landsat 7, only on path 29) versus ET_rF produced from the baseline model run 1 for the central Nebraska analysis area for year 2002.

of ET rates from individual fields. Statistical summaries are presented in a later section.

Agreement between runs 2–5 and baseline run 1 were even more improved for the month of July (**Figure 13**) for the Nebraska study area. July is the month where most crops have attained full ground cover and ET_rF rates are near their maximum

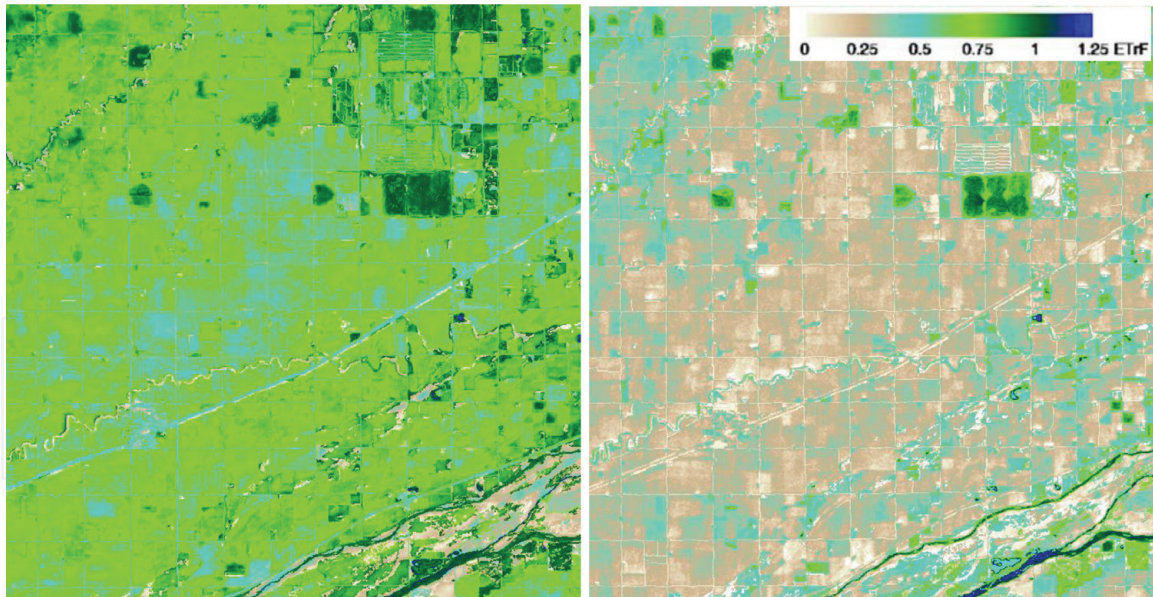


Figure 11.
ET,F for May 2, 2002 path 30 (Left) and ET,F for May 3, 2002 path 29 (Right).

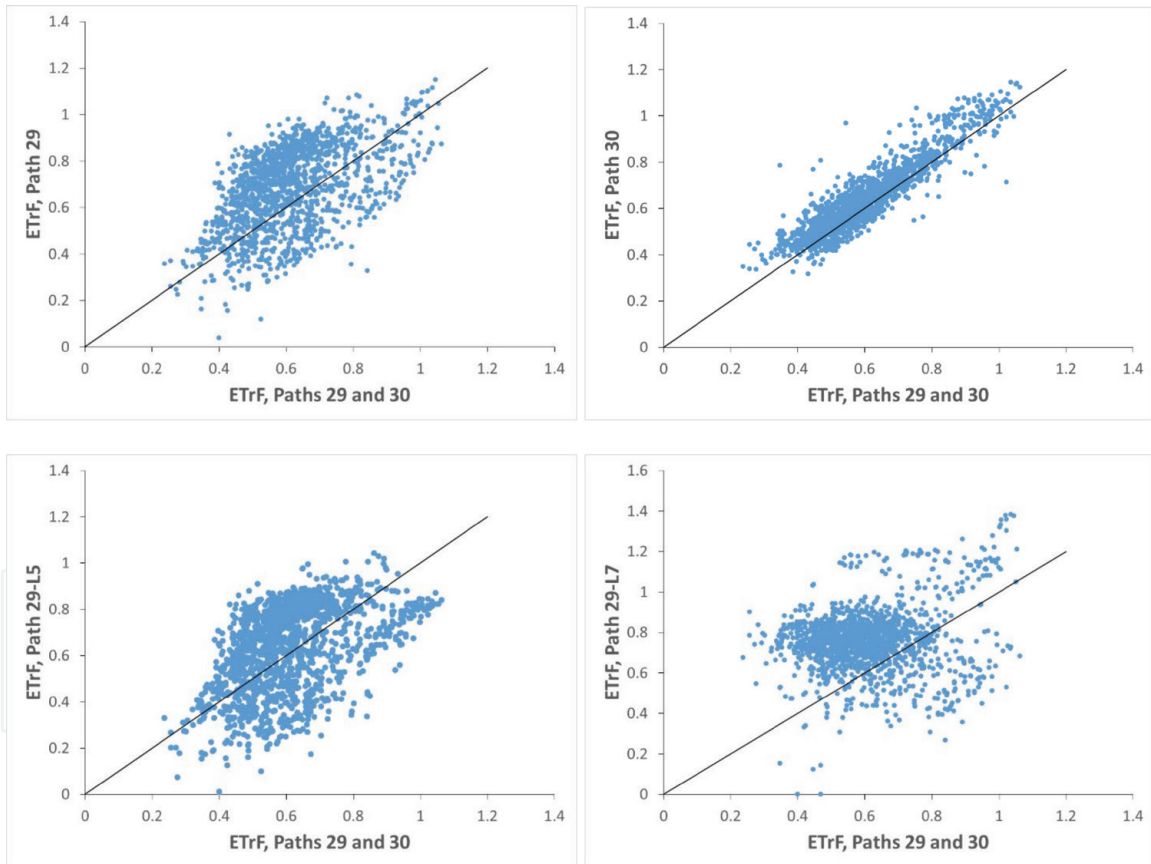


Figure 12.
Plots of average integrated ET,F for June from model run 2 (two Landsats on path 29), run 3 (two satellites on path 30), run 4 (Landsat 5, only on path 29), and run 5 (Landsat 7, only on path 29) versus ET,F produced from the baseline model run 1 for the central Nebraska analysis area for year 2002.

values. July is also the month having the highest total ET amounts, as summarized later in the statistics section. For July, only run 3 had substantial disagreement, where images from both Landsats for path 30 only were utilized in the time integration. That disagreement may have stemmed from differences in evaporation amounts from fields having low vegetation cover due to differences in antecedent rainfall.

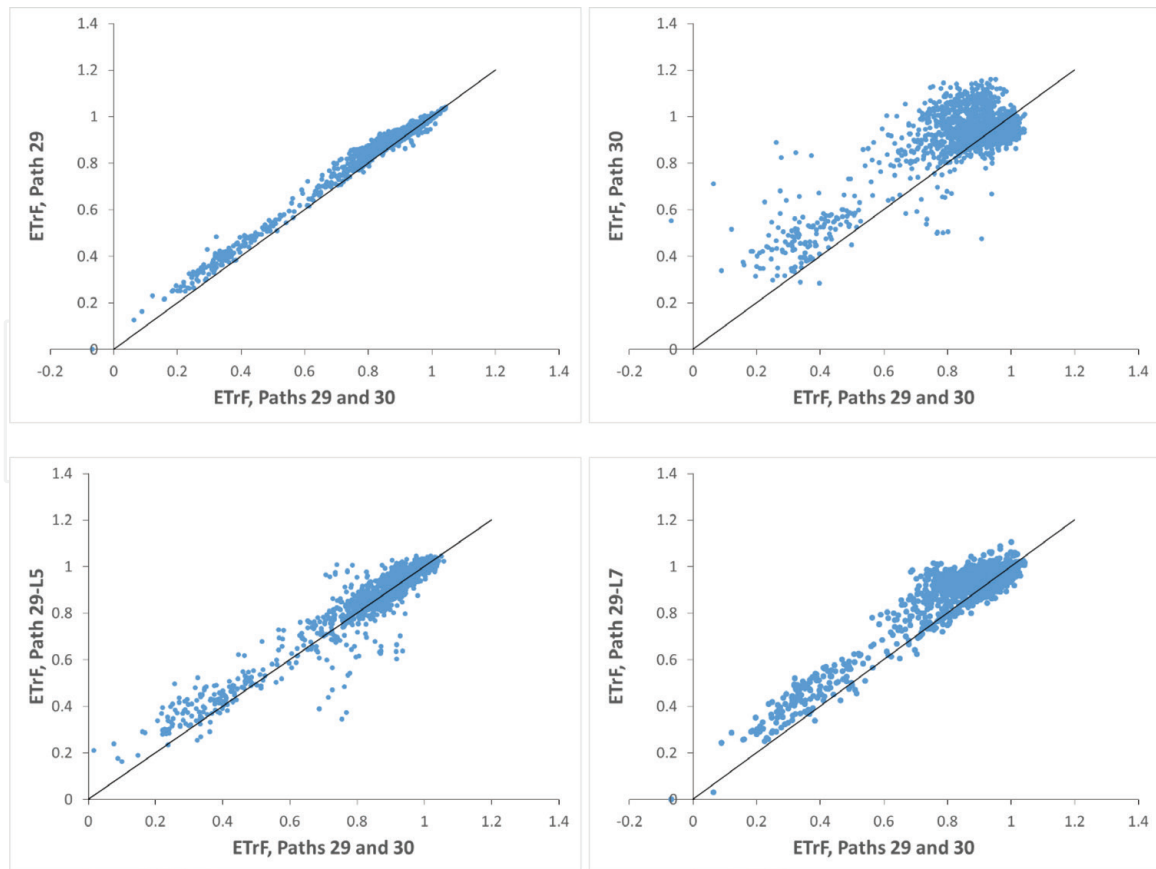


Figure 13. Plots of average integrated $ET_{r,F}$ for July from model run 2 (two Landsats on path 29), run 3 (two satellites on path 30), run 4 (Landsat 5, only on path 29), and run 5 (Landsat 7, only on path 29) versus $ET_{r,F}$ produced from the baseline model run 1 for the central Nebraska analysis area for year 2002.

Relatively, good agreement between runs 2–5 and baseline run 1 occurred for the month of August (**Figure 14**) for the Nebraska study area. As for July, August is a month where most crops have full ground cover and monthly $ET_{r,F}$ rates are near their maximum values. The relatively good agreement between time-integrated ET using fewer available images and the baseline condition most likely stems from the relatively ‘flat’ nature of the $ET_{r,F}$ curve during the July–early September period, where change in $ET_{r,F}$ is gradual. Therefore, the spline function tended to produce similar spline shapes among the various collections of $ET_{r,F}$ images and image dates.

Total monthly ET averaged over the 1500 sample points is plotted in **Figure 15** and monthly $ET_{r,F}$ is plotted in **Figure 16** for months of May through September for the Nebraska study area. Except for May and model run 5 (path 29 with only Landsat 7), values of ET and $ET_{r,F}$, when averaged over a large number of fields, produced relatively similar and consistent results. Differences in ET for the month of May have been previously discussed. The relatively good agreement in ET when averaged over a large area is of interest for ET data uses such as ground water depletion studies and river depletion studies, where ET integrated over areas larger than a single field is of value.

3.3 Growing season ET

Growing season (April–October) ET produced by the time-integration is plotted in **Figure 17** for the Idaho study area for runs 2, 3, and 4 versus run 1. Agreement was strongest between run 1 and runs 3 and 4. Growing season ET produced from path 39 images, only, tended to underestimate ET according to the run 1 basis by about 8% on average. Statistics are summarized later in **Table 3**.

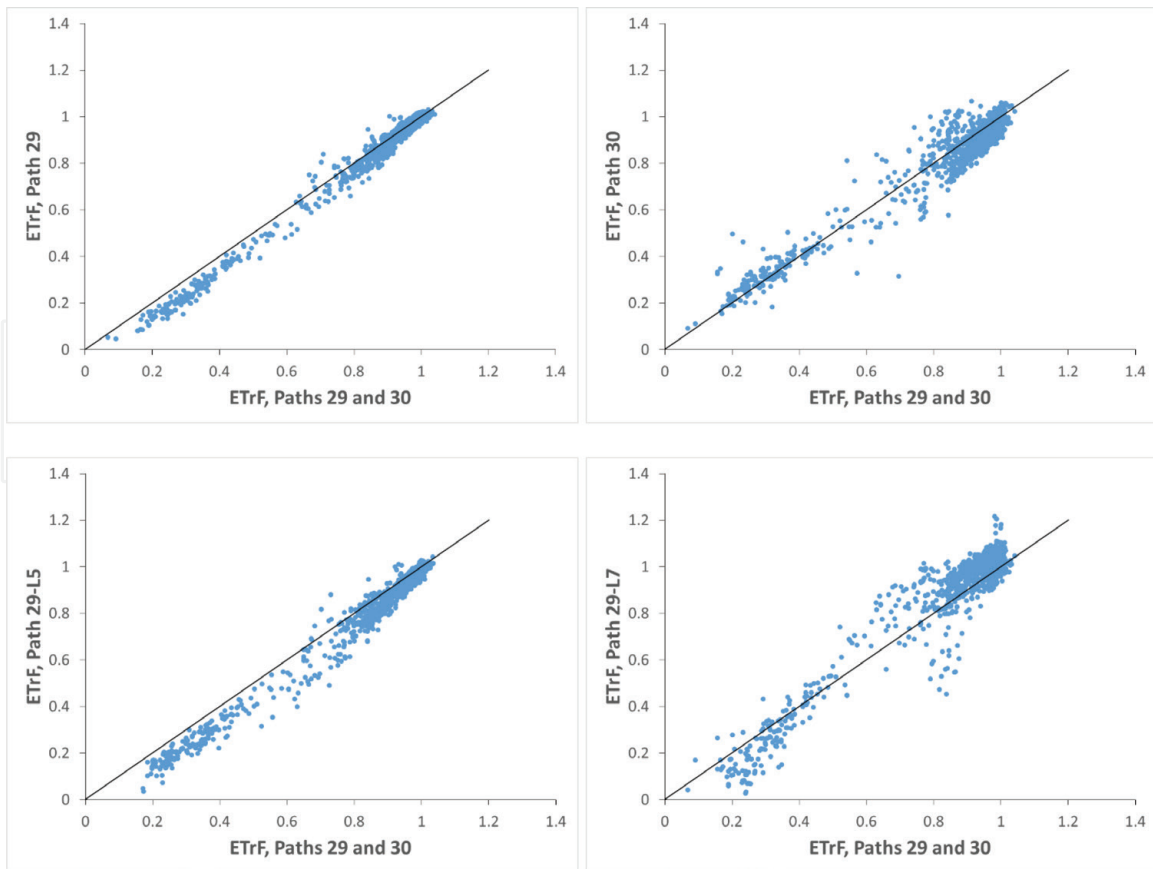


Figure 14. Plots of average integrated ET,F for August from model run 2 (two Landsats on path 29), run 3 (two satellites on path 30), run 4 (Landsat 5, only on path 29), and run 5 (Landsat 7, only on path 29) versus ET,F produced from the baseline model run 1 for the central Nebraska analysis area for year 2002.

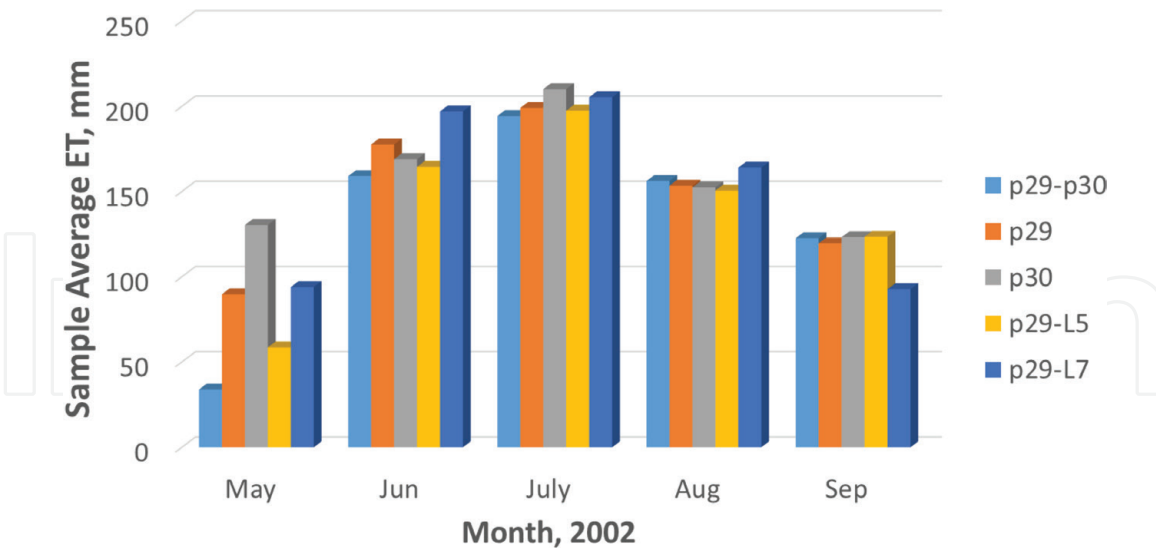


Figure 15. Monthly ET averaged from the 1500 sample pixels for the Nebraska study area for the five time-integration runs.

Growing season (March–September) ET produced by the time-integration is plotted in **Figure 18** for the Nebraska study area for runs 3, 2, and 5 versus run 1. Agreement was strongest between baseline run 1 and run 2 that used images from both Landsats from path 29 only. Growing season ET produced from path 29 using only Landsat 7 images only had the worse correlation with $r^2 = 0.64$. Growing season ET produced from path 29 images, tended to overestimate ET according to the baseline run 1 by about 19% on average.

3.4 Statistical summaries

Table 3 summarizes monthly average ET for the four time-integration runs for the Idaho study area and root mean square error (RMSE) for the 1500 sampled fields. RMSE was relatively high for run 2 (both satellites for path 39 only),

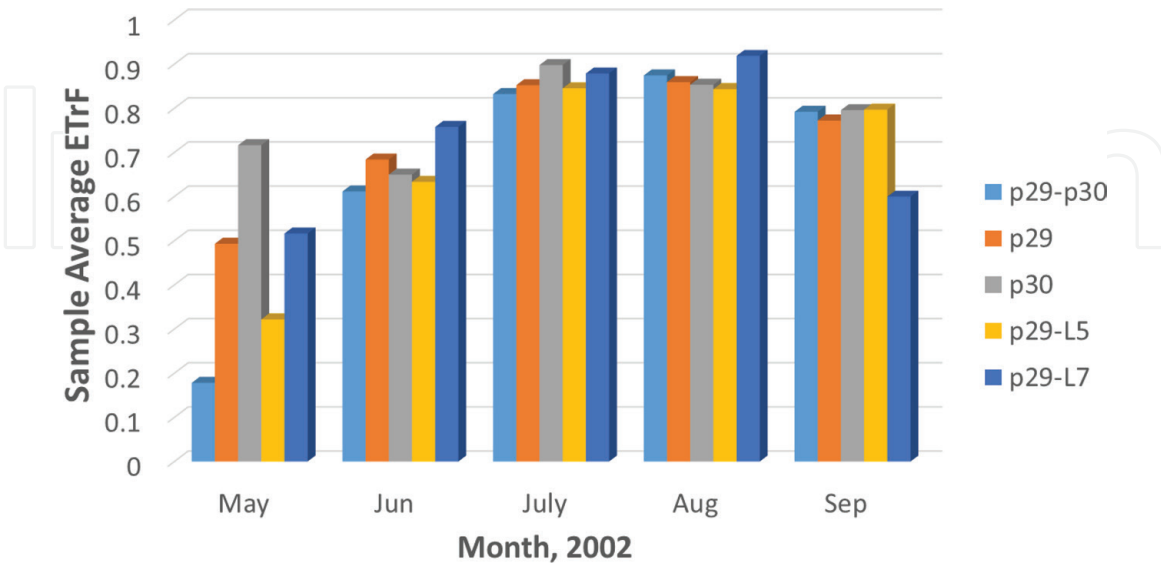


Figure 16. Monthly ET_r averaged over the 1500 sample pixels for the Nebraska study area for the five time-integration runs.

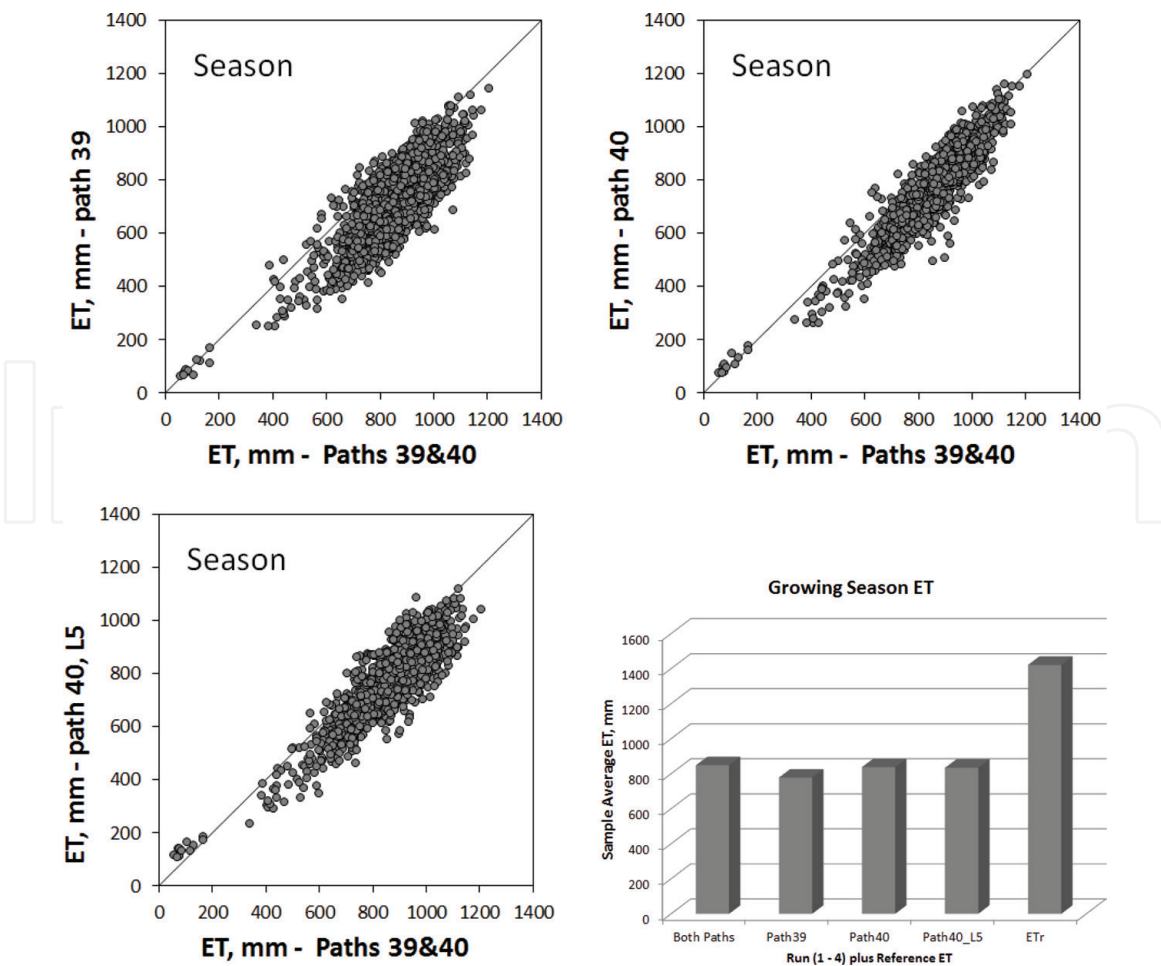


Figure 17. ET for April–October growing season for 1500 sampled locations for the Idaho study area for the time-integration runs 2, 3, and 4 versus run 1 and (lower right) averages over all 1500 sampled fields. Also shown in the lower right is reference ET summed over the April–October period.

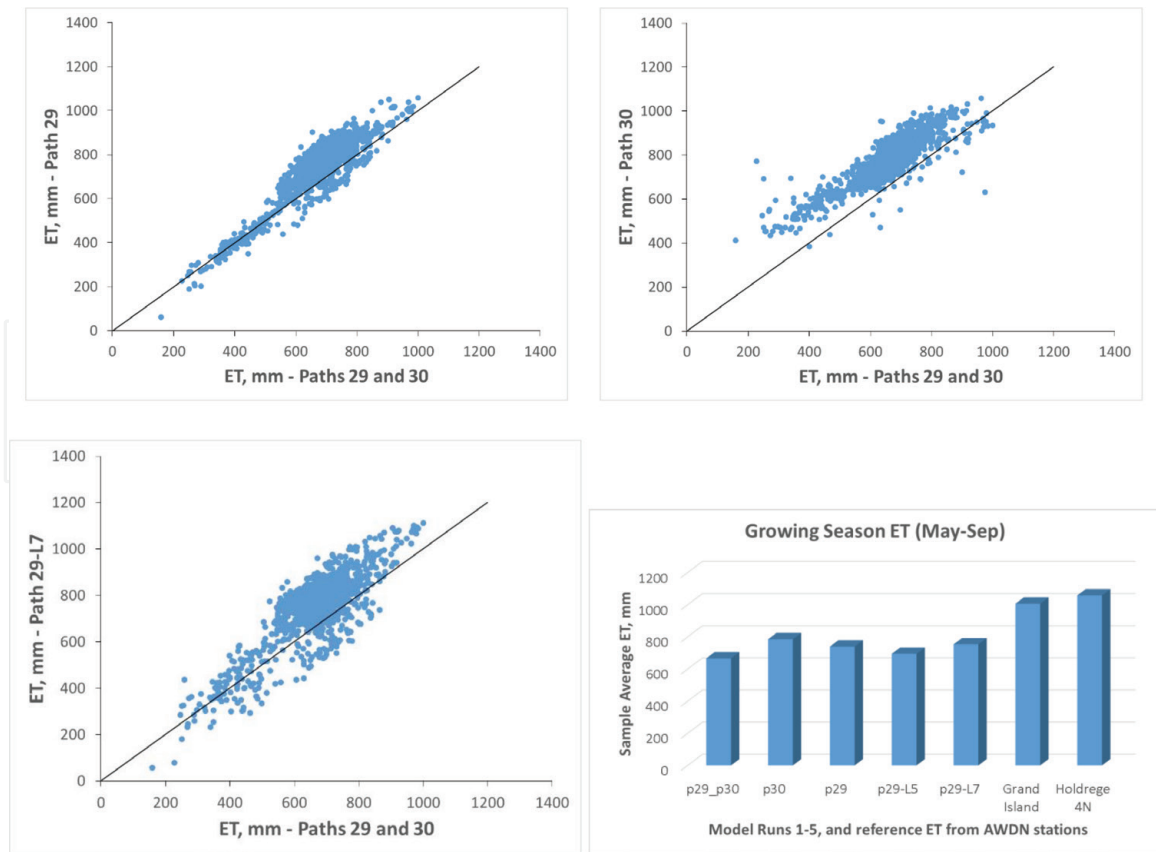


Figure 18. Total ET for May–September growing season of 2002 for 1500 sampled locations for the Nebraska study area for time-integration model runs 3, 2, and 5 versus model run 1. Also shown in the lower right is total growing season ET averaged over all samples and reference ET from two AWDN stations (right two columns).

		Average ET, RMSE, and Total ET _r are in mm—Year 2000						
		April	May	June	July	August	Sept	Oct
Average	Both paths	40	99	173	225	159	99	54
	Path 39	35	79	165	204	153	98	43
	Path 40	33	94	187	233	165	80	46
	Path 40_L5 only	37	93	187	233	167	84	33
RMSE	Both paths	0	0	0	0	0	0	0
	Path 39	34	48	18	76	51	19	23
	Path 40	19	41	23	55	41	35	12
	Path 40_L5 only	25	40	23	54	43	37	27
% error*	Both paths	0	0	0	0	0	0	0
	Path 39	20	24	7	29	23	11	21
	Path 40	11	21	9	21	18	21	11
	Path 40_L5 only	14	20	9	21	19	22	24
ET_r		174	200	274	265	227	171	111

*% error is RMSE error relative to ET_r.

Table 3. Average monthly ET over the 1500 sampled fields in the Idaho study area for the four runs and RMSE, percentage error and reference ET.

exceeding 20% of reference ET for 5 of 7 months. RMSE for runs 3 and 4 had less error than run 2 for 2 months, even though run 4 utilized only seven image dates (from Landsat 5 and path 40) in the integration. This indicates the importance of timing of images to identify key inflection points in the ET_rF curves and to capture special events such as wetting events from irrigation and rain or from water stress or cuttings, as in the case of alfalfa hay. **Table 4** summarizes growing season comparisons for ET among the four runs. The runs that used images from path 40 only compared to within 2%, when averaged over all 1500 fields, to the baseline run. This outcome is likely due to the timing of path 40 images relative to the combined run as compared to path 39. This shows the high value of a high density of image dates so that important inflection points in ET_rF curves can be obtained.

Table 5 provides monthly average ET, RMSE, percentage error (RMSE error in relation to ET_r), and total monthly reference ET for the 1500 pixel sample locations in the Nebraska study area. RMSE was high for all model runs for May and June, exceeding 19%, with a maximum RMSE of 104% for model run 2 for May. Model run 2 (both Landsats from path 30 only) had lower error for June compared to May

	ET (mm)	% Diff	ET_rF
Both paths	849	0.00	0.60
Path 39	778	8.30	0.50
Path 40	838	1.25	0.53
Path 40_L5	834	1.74	0.53
ET_r	1422		

Table 4. Growing season ET (April–October 2000) averaged over 1500 sampled fields in the Idaho study area for the four runs and percent differences from the base run 1.

		Average ET, RMSE, and Total ET_r are in mm—Year 2002				
		May	June	July	August	Sept
Average	Both paths	34	159	194	156	123
	Path 30	130	169	210	152	123
	Path 29	90	178	199	153	120
	Path 29_L5 only	59	164	197	151	123
	Path 29_L7 only	94	197	205	164	93
RMSE	Both paths	0	0	0	0	0
	Path 30	104	19	31	10	6
	Path 29	61	45	8	6	7
	Path 29_L5 only	52	45	14	8	8
	Path 29_L7 only	64	63	19	14	32
% error*	Both paths	0	0	0	0	0
	Path 30	56	7	13	6	4
	Path 29	33	17	3	3	4
	Path 29_L5 only	28	17	6	5	5
	Path 29_L7 only	35	24	8	8	29
ET_r (mm)		184	259	232	173	158

*Percentage error is RMSE error relative to ET_r .

Table 5. Average monthly ET, RMSE, percentage error, and total monthly reference ET for the 1500 pixel sample locations for the Nebraska study area.

or July, which emphasizes the impact of the timing of the images used. For path 30, image date June 28, 2002 had large areas of clouds masked out, which were filled in using the next available image date in time in the spline function. This underscores the importance of timing of images to identify key inflection points in the $ET_{r,F}$ curves and to capture special events such as wetting events from irrigation and rain or from water stress or cuttings, as in the case of alfalfa hay.

4. Conclusions

In this study, monthly and growing season ET maps were derived by interpolating $ET_{r,F}$ produced by METRIC for processed images and then multiplying, on a daily basis, by a reference ET_r for each day to account for day-to-day variation in ET caused by weather fluctuations. The objective of the study was to explore the change in estimates for ET over complete growing seasons and for monthly periods when more frequent or less frequent Landsat imagery was available. The study was implemented by conducting a series of METRIC applications for a Landsat WRS path overlap area in southern Idaho (paths 39 and 40) during year 2000 and for a WRS path overlap area in central Nebraska (paths 29 and 30) during year 2002 when two fully functioning satellites, Landsat 5 and Landsat 7, were in orbit. During those years, Landsat 5 (L5) and Landsat 7 (L7) passed over the overlap areas twice, each, per 16 day period, providing four imaging opportunities every 16 days. The frequency of imagery was sparsened by removing imagery from one path or the other and by removing imagery from one satellite or the other. Monthly and seasonal ET were recomputed with the sparsened image series and compared with the baseline data. Idaho is a relatively 'clear' area, so that this analysis represents a somewhat 'optimistic' scenario, and Nebraska represents the more cloud-prone parts of the USA including the Midwestern states.

The higher frequency imagery used in baseline run 1 was more able to capture the impacts of harvest and regrowth of alfalfa on the $ET_{r,F}$ rate in the Idaho study area. Sparsened runs missed some of the alfalfa regrowth cycles. Run 4 that used only 7 image dates generated smoother $ET_{r,F}$ curves due to the more sparse data points. The smoother curve tended to average out variation in $ET_{r,F}$ caused by variation in water availability or variation in evaporation from soil following irrigation or precipitation wetting events. Time-integration runs 5, 6, and 7, which would have represented three additional replicates of a single satellite having 16-day revisit, via combinations of path 40 with Landsat 7 and path 39 with Landsat 5 and path 39 with Landsat 7, were not possible to implement in the Idaho study area due to too few images per combination to apply the $ET_{r,F}$ interpolation process. This severe limitation on application of those scenarios emphasizes the need to maintain two Landsat satellites in orbit and ideally to have four-day revisit times.

Similar results occurred for the Nebraska study area, where very large differences between runs occurred for the month of May. May is a period of very low-to-low vegetation amounts for many fields and is therefore more prone to varying wetness of images caused by evaporation from bare soil following precipitation events.

Integrated ET from individual fields deviated relatively widely, which would be a concern for those individual water rights holders and managers of water rights or pumping permits. However, ET and $ET_{r,F}$ averaged over a large number of fields yielded relatively similar and consistent values. Limiting the data source to one path with two satellites impacted the monthly integrations and growing season ET produced from one path only. ET based on a single path only underestimated ET according to the run 1 basis by about 8% on average for the Idaho study area and by about 20% for the Nebraska study area.

Error in monthly ET was relatively high when image availability was limited to about one-half of the full 21 image data set, exceeding 20% of reference ET for 5 of 7 months in the Idaho study area. This indicates the importance of timing of images to identify key inflection points in the ET_rF curves and to capture special events such as wetting events from irrigation and rain or from water stress or cuttings, as in the case of forage crops.

Results suggest that a four-day revisit time as represented by the full-run (run 1) of these analyses provides robustness in development of time-integrated ET estimates over months and growing seasons and is a valuable backstop for mitigation of clouded images over extended periods.

Conflict of interest

The authors declare no conflict of interest.

Author details

Ricardo Trezza^{1*}, Richard G. Allen¹, Ayse Kilic², Ian Ratcliffe²
and Masahiro Tasumi³


¹ Kimberly Research and Extension Center, University of Idaho, Kimberly, Idaho, USA

² Civil Engineering/SNR, University of Nebraska, Lincoln, Nebraska, USA

³ University of Miyazaki, Miyazaki, Japan

*Address all correspondence to: rtrezza@uidaho.edu

IntechOpen

© 2018 The Author(s). Licensee IntechOpen. This chapter is distributed under the terms of the Creative Commons Attribution License (<http://creativecommons.org/licenses/by/3.0>), which permits unrestricted use, distribution, and reproduction in any medium, provided the original work is properly cited. 

References

- [1] Kustas WP, Norman JM. Use of remote sensing for evapotranspiration monitoring over land surfaces. *Hydrological Sciences Journal*. 1996;**41**:495-515
- [2] Bastiaanssen WGM. Remote Sensing in Water Resources Management: The State of the Art. Sri Lanka: IWMI; 1998
- [3] Courault D, Seguin B, Olioso A. Review on estimation of evapotranspiration from remote sensing data: From empirical to numerical approaches. *Irrigation and Drainage Systems*. 2005;**19**:223-249
- [4] Kalma JD, McVicar TR, McCabe MF. Estimating land surface evaporation: A review of methods using remotely sensed surface temperature data. *Surveys in Geophysics*. 2008;**29**:421-469
- [5] Kamble B, Kilic A, Hubbard K. Estimating crop coefficients using remote sensing-based vegetation index. *Remote Sensing*. 2013;**5**:1588-1602
- [6] Nagler P, Glenn E, Nguyen U, Scott R, Doody T. Estimating riparian and agricultural actual evapotranspiration by reference evapotranspiration and MODIS enhanced vegetation index. *Remote Sensing*. 2013;**5**:3849-3871
- [7] Bastiaanssen WGM. Regionalization of surface flux densities and moisture indicators in composite terrain: A remote sensing approach under clear skies in mediterranean climates. Ph.D. Thesis. Den Haag, The Netherlands: CIP Data Koninklijke Bibliotheek; 1995. p. 273
- [8] Trezza R. Evapotranspiration using a satellite-based surface energy balance with standardized ground control. PhD Dissertation. Logan, Utah: Utah State University; 2002
- [9] Tang R, Zhao-Liang L, Tang B. An application of the Ts-VI triangle method with enhanced edges determination for evapotranspiration estimation from MODIS data in arid and semi-arid regions. *Remote Sensing of Environment*. 2010;**114**:540-551
- [10] Anderson M, Allen RG, Morse A, Kustas WP. Use of Landsat thermal imagery in monitoring evapotranspiration and managing water resources. *Remote Sensing of Environment*. 2012;**122**:50-65
- [11] Allen RG, Pereira LS, Raes D, Smith M. *Crop Evapotranspiration: Guidelines for Computing Crop Water Requirements; Irrigation and Drainage Paper 56*. Rome, Italy: United Nations FAO; 1998. p. 300
- [12] Allen RG, Tasumi M, Morse A, Trezza R, Kramber W, Lorite I, et al. Satellite-based energy balance for mapping evapotranspiration with internalized calibration (METRIC)—Applications. *ASCE Journal of Irrigation and Drainage Engineering*. 2007;**133**:395-406
- [13] Allen RG, Tasumi M, Trezza R. Satellite-based energy balance for mapping evapotranspiration with internalized calibration (METRIC)—Model. *ASCE Journal of Irrigation and Drainage Engineering*. 2007;**33**:380-394
- [14] Chavez JL, Neale CMU, Prueger JH, Kustas WP. Daily evapotranspiration estimates from extrapolating instantaneous airborne remote sensing ET values. *Irrigation Science*. 2008;**27**:67-81
- [15] Singh R, Liu S, Tieszen L, Suyker A. Estimating seasonal evapotranspiration from temporal satellite images. *Irrigation Science*. 2011;**30**:303-313

- [16] Mohamed YA, Bastiaanssen W, Savenje H. Spatial variability of evaporation and moisture storage in the swamps of the upper Nile studied by remote sensing techniques. *Journal of Hydrology*. 2004;**289**:145-164
- [17] Bastiaanssen WGM, Menenti M, Feddes RA, Holtslag AAM. A remote sensing surface energy balance algorithm for land (SEBAL): 1. Formulation. *Journal of Hydrology*. 1998;**212-213**:198-212
- [18] Bashir M, Hata T, Tanakamaru H, Abdelhadi A. Satellite-based energy balance model to estimate seasonal evapotranspiration for irrigated sorghum: A case study from the Gezira scheme, Sudan. *Hydrology and Earth System Sciences*. 2008;**12**:1129-1139
- [19] Olioso A, Chauki H, Courault D. Estimation of evapotranspiration and photosynthesis by assimilation of remote sensing data into SVAT models. *Remote Sensing of Environment*. 1999;**68**:341-356
- [20] Dhungel R, Allen R, Trezza R, Robison C. Comparison of latent heat flux using aerodynamic methods and using the Penman-Monteith method with satellite-based surface energy balance. *Remote Sensing*. 2014;**6**(9):8844-8877
- [21] Allen RG, Tasumi M, Morse A, Trezza R. A Landsat-based energy balance and evapotranspiration model in Western US water rights regulation and planning. *Journal of Irrigation and Drainage Engineering*. 2005;**19**:251-268
- [22] Bastiaanssen WGM, Pelgrum H, Wang J, Ma Y, Moreno J, Roerink GJ, et al. The surface energy balance algorithm for land (SEBAL): Part 2 validation. *Journal of Hydrology*. 1998;**212-213**:213-229
- [23] Allen RG, Tasumi M, Trezza R. Benefits from tying satellite-based energy balance to reference evapotranspiration. In: D'Urso G, Jochum A, Moreno J, editors. *Earth Observation for Vegetation Monitoring and Water Management: Naples, Italy, 10-11 November 2005*. Vol. 2005. College Park, MD, USA: American Institute of Physics. pp. 127-137
- [24] ASCE-EWRI. The ASCE Standardized Reference Evapotranspiration Equation; ASCE-EWRI Standardization of Reference Evapotranspiration Task Committee Report. Reston, VA, USA: ASCE; 2005. p. 216
- [25] Tasumi M, Allen RG, Trezza R, Wright JL. Satellite-based energy balance to assess within-population variance of crop coefficient curves. *ASCE Journal of Irrigation and Drainage Engineering*. 2005;**131**:94-109